The nebulin repeat protein Lasp regulates I-band architecture and filament spacing in myofibrils

Isabelle Fernandes and Frieder Schöck

Department of Biology, McGill University, Montreal, Quebec, Canada H3A 1B1

Mutations in nebulin, a giant muscle protein with 185 actin-binding nebulin repeats, are the major cause of nemaline myopathy in humans. Nebulin sets actin thin filament length in sarcomeres, potentially by stabilizing thin filaments in the I-band, where nebulin and thin filaments coalign. However, the precise role of nebulin in setting thin filament length and its other functions in regulating power output are unknown. Here, we show that Lasp, the only member of the nebulin family in *Drosophila melanogaster*, acts at two distinct sites in the sarcomere and controls thin filament length with just two nebulin repeats. We found that Lasp localizes to the Z-disc edges to control I-band architecture and also localizes at the A-band, where it interacts with both actin and myosin to set proper filament spacing. Furthermore, introducing a single amino acid change into the two nebulin repeats of Lasp demonstrated different roles for each domain and established Lasp as a suitable system for studying nebulin repeat function.

Introduction

Nemaline myopathy (NM) is one of the most common congenital skeletal muscle diseases. Mutations in the nebulin gene account for the majority of cases and, to date, 64 different mutations have been reported in nebulin (Pelin et al., 1999; Lehtokari et al., 2006; Wallgren-Pettersson et al., 2011). Therefore, understanding nebulin function in muscles will shed light on the underlying causes of NM.

Striated muscles consist of myofibrils, which are composed of a series of sarcomeres, the smallest contractile unit of muscles. Each sarcomere is bordered by Z-discs, to which the actin thin filaments are anchored. Thin filaments interdigitate with myosin thick filaments, which are anchored in the middle of the sarcomere at the M-line. Together with the elastic support protein titin, the sliding of thin and thick filaments generates the contractile force of muscles (Sparrow and Schöck, 2009). Nebulin is a giant actin-binding protein expressed in skeletal muscle, which is composed of 185 copies of a 35–amino acid sequence referred to as nebulin repeat (Pappas et al., 2011; Ottenheijm et al., 2012). These repeats contain a conserved actin-binding SDxxYK motif (Labeit and Kolmerer, 1995). Immuno-EM has revealed that a single nebulin molecule spans the thin filaments with its C-terminal part anchored at the Z-disc and its N-terminal part directed toward the thin filament pointed end, with each nebulin repeat likely interacting with a single monomer of actin (Wright et al., 1993). Nebulin-deficient mice have shorter thin filaments resulting in shorter sarcomeres (Bang et al., 2006; Witt et al., 2006). Nebulin was originally believed to act as a molecular ruler, but this model is no longer favored because a smaller nebulin molecule with 59 nebulin repeats can specify thin filament length in skeletal myocytes as well as full-length nebulin does (Pappas et al., 2010). Nebulin is now proposed to regulate thin filament length either through binding the barbed end capping protein CapZ (Pappas et al., 2008) or by stabilizing actin thin filaments through binding of multiple nebulin repeats along the I-band (Pappas et al., 2010; Gokhin and Fowler, 2013).

In vertebrates, the giant protein nebulin is the founding and largest member of a family of actin-binding proteins that also includes N-RAP (nebulin-related anchoring protein), nebulette, Lasp-1, and Lasp-2 (LIM and SH3 protein). These other members of the nebulin family contain significantly fewer nebulin repeats and are more widely expressed (Pappas et al., 2011). All of them except N-RAP have an SH3 domain at the C terminus, whereas N-RAP, Lasp-1, and Lasp-2 have a LIM domain at the N terminus, which is not present in nebulin and nebulette. Nebulette is a cardiac-specific family member that localizes strictly to the Z-disc and is associated with dilated cardiomyopathy

Correspondence to Frieder Schöck: frieder.schoeck@mcgill.ca

Abbreviations used in this paper: BWM, body wall muscle; IFM, indirect flight muscle; NM, nemaline myopathy; TDT, tergal depressor of the trochanter.
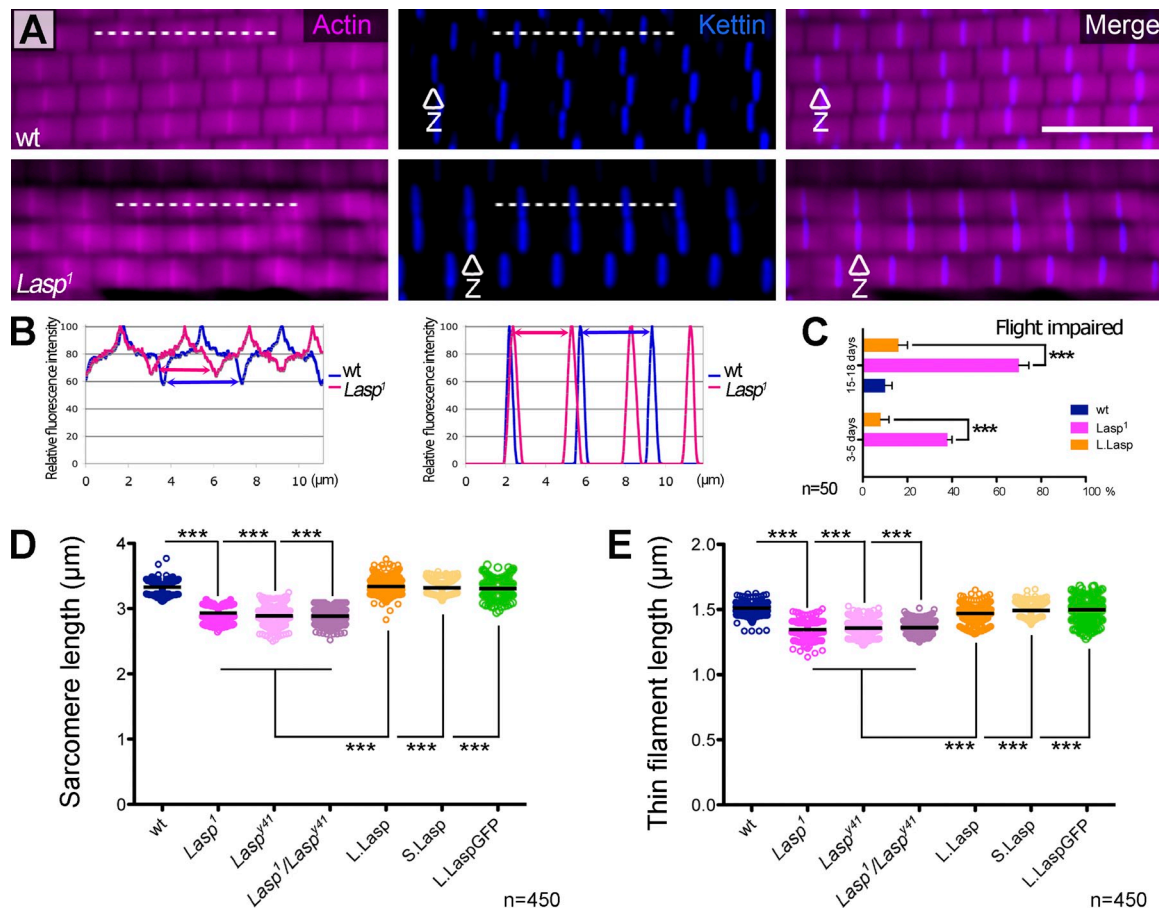
Figure 1. ***Lasp¹* mutants have shorter sarcomere and thin filament length.** (A) Wild type (top) and *Lasp¹* mutant (bottom) of IFM myofibrils stained with phalloidin (magenta) to label actin thin filaments and with anti-Kettin (blue) to mark Z-discs (arrowheads). Staining reveals an ordered pattern of myofibrils displaying a wild-type organization. Bar, 5 µm. (B) Graphs represent actin and Kettin grayscale intensity across the dashed line on the corresponding top panel. *Lasp¹* mutants (pink line) have shorter sarcomeres and thin filaments compared with wild type (blue line). (C) Flight assays on 3–5- or 15–18-d-old adults demonstrate that *Lasp¹* mutant flies have reduced flight ability that can be rescued by reexpressing L.Lasp in *Lasp¹*. The wild-type bar in 3–5-d-old flies is not visible because 0% of flies are flight impaired. Error bars indicate SD. (D) Quantification of sarcomere length. (E) Quantification of thin filament length. *Lasp¹*, *Lasp^y41*, and *Lasp¹*/*Lasp^y41* have shorter sarcomere and thin filament length. Reexpressing L.Lasp, S.Lasp, or L.LaspGFP with Mef2-Gal4 in *Lasp¹* rescues sarcomere and thin filament length. ***, P < 0.0001. Adult flies in A, B, D, and E were 3 d old.

when mutated in humans (Millevoi et al., 1998; Pappas et al., 2011). Lasp-2 is a shorter splice variant of nebulette with only three nebulin repeats that localizes in striated muscles to Z-discs (Zieseniss et al., 2008). N-RAP also localizes to Z-discs and together with α-actinin helps organize Z-disc structure (Lu et al., 2003). Finally, Lasp-1 has only two nebulin repeats and no described function in muscles: Lasp-1 knockout mice are viable with no overt phenotypic abnormalities (Chew et al., 2008).

In *Drosophila melanogaster*, *Lasp* encodes the single member of the nebulin family and exhibits homology to human Lasp-1. Lasp modulates the actin cytoskeleton in the germline and, similar to other nebulin family proteins, Lasp binds actin in vitro (Lee et al., 2008; Suyama et al., 2009). Analyzing Lasp will contribute to the understanding of all nebulin family members because Lasp-like proteins are found in at least one copy in all vertebrates and invertebrates, from sponges to humans, indicating that the evolution of nebulin repeat–containing proteins started with a Lasp-like protein (Nichols et al., 2006; Björklund et al., 2010).

Here we show that Lasp carries out the main function that nebulin fulfills in vertebrates, the setting of thin filament length.

In addition, Lasp modulates I-band architecture by interacting with titin family proteins and α-actinin and affects filament packing by interacting with both actin and myosin. These phenotypes are mediated by a dual localization of Lasp to the Z-disc edges and at the A-band. Physiologically, these defects result in substantially reduced crawling and flying ability. Importantly, a single amino acid change in the actin-binding motif of nebulin repeat 1 and 2 demonstrates different functions for each domain. Therefore, our work establishes Lasp as a model system for understanding the mechanism of nebulin repeat function.

Results

Thin filaments are shorter in *Lasp* mutants

One of the main functions of nebulin is the establishment of thin filament length (McElhinny et al., 2005; Bang et al., 2006; Witt et al., 2006; Ottenheijm et al., 2009). We therefore asked if the single nebulin family member in *Drosophila*, Lasp, also regulates thin filament length, even though Lasp has only two nebulin repeats. We first examined the indirect flight muscle (IFM)
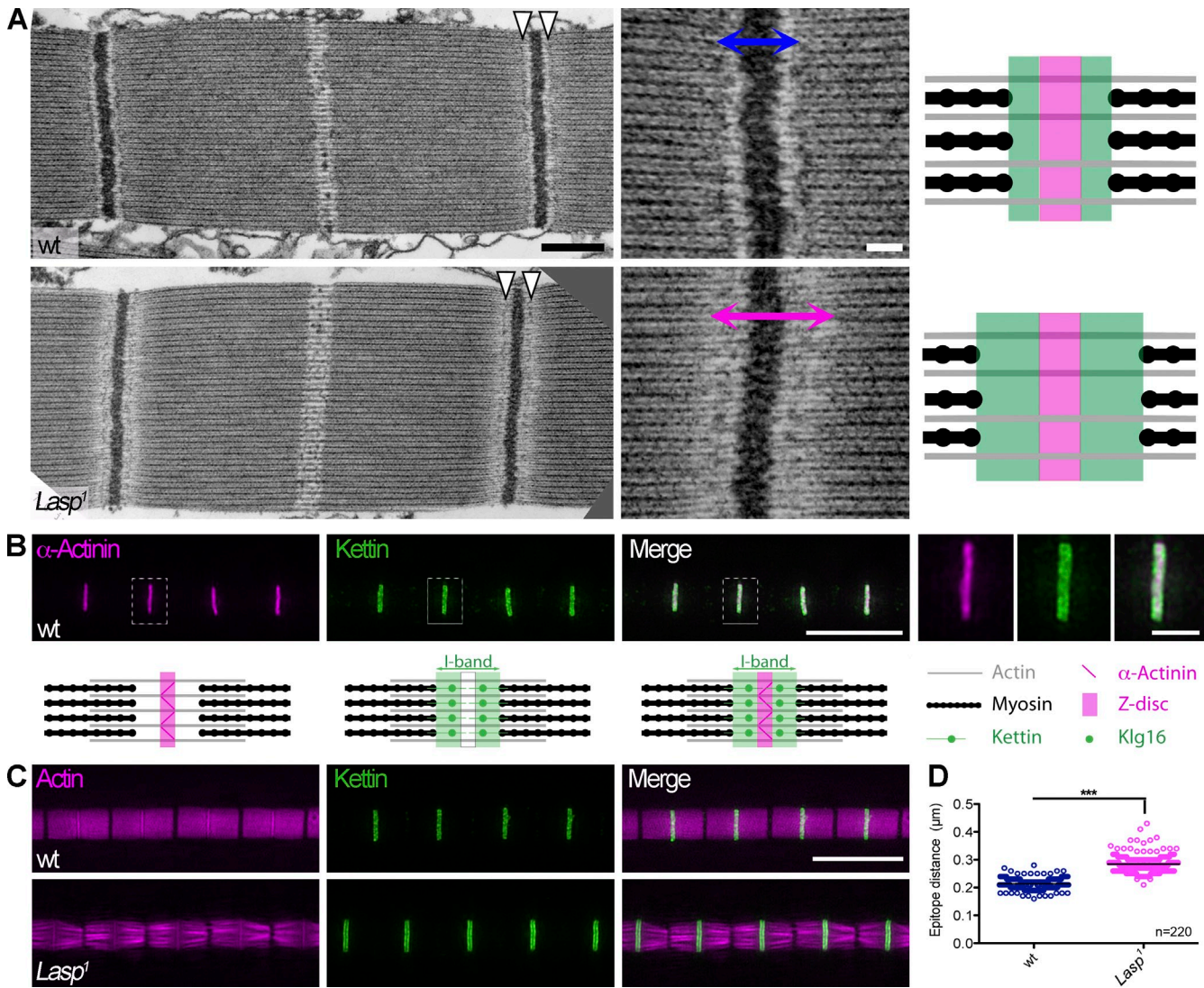
Figure 2. **I-band architecture is altered in *Lasp¹* mutants.** (A) EM of longitudinal sections of IFM myofibrils from 18-d-old wild-type (top) and *Lasp¹* mutant flies (bottom). Sarcomeres are shorter, but no gross structural defects are visible in *Lasp¹* mutants. Close-up view of Z-disc shows an enlargement of the I-band in *Lasp¹* mutants in 54% of sarcomeres (*n* = 49). I-band width is indicated by blue and pink arrows. White arrowheads mark a row of electron-dense material on both sides of the Z-disc, which is less dense in *Lasp¹* mutants. Schematic representation of the structure is shown in the side panel. Bars: (left) 500 nm; (right) 100 nm. (B) Structured illumination superresolution microscope images of wild-type IFM myofibrils stained with anti–α-actinin (magenta) and anti-Kettin (green). Kettin Klg16 signal now resolves as two lines on both sides of the Z-disc core protein α-actinin. Schematic representation of the staining is shown in the bottom panel. (C) Wild-type (top) and *Lasp¹* (bottom) IFM myofibrils stained with phalloidin (magenta) and anti-Kettin (green). Note that actin thin filament packing shows some defects in *Lasp¹* mutant myofibril. Bars: (B and C) 5 µm; (B, right) 1 µm. (D) Quantification of distance between Kettin Klg16 epitopes. ***, P < 0.0001. Data in B–D are from 5-d-old adults.

of *Lasp¹* null mutant adults stained for actin and Kettin, a titin family member used as a Z-disc marker, by confocal microscopy. No gross defects can be observed, but sarcomeres as well as thin filaments from *Lasp¹* mutants were 12% shorter than those of wild type (Fig. 1, A, B, D, and E). We also analyzed an independent *Lasp* null mutant allele, *Lasp^y41* (Suyama et al., 2009), which shows the same reduction in sarcomere and thin filament length both homozygously and transheterozygously (Fig. 1, D and E). These reductions are in the same range as those observed in nebulin-deficient mice (Bang et al., 2006; Witt et al., 2006).

FlyBase annotates four different Lasp isoforms with molecular masses of 32.2, 56, 71.9, and 74.2 kD. The 71.9- and 74.2-kD isoforms are the most common ones in muscles we have analyzed (see Fig. S3). All isoforms have a LIM domain, nebulin repeats, and an SH3 domain and differ only in the length of the linker region between nebulin repeat 2 and the SH3 domain. Expressing the long isoform of Lasp, either carrying an N-terminal Flag and His tag (called L.Lasp) or a C-terminal GFP tag (L.LaspGFP) with Mef2-Gal4, a muscle-specific driver, in a *Lasp¹* mutant background rescues sarcomere and thin filament length (Fig. 1, D and E). Therefore, Lasp is specifying thin filament and sarcomere length, and our rescue assay is suitable to test the function of transgenes expressing different mutant Lasp proteins. We then tested the 56-kD isoform called S.Lasp, which we cannot detect in IFM. S.Lasp also rescues fully (Fig. 1, D and E),

indicating that in IFM conserved domains are more important for muscle function than the linker region. Because of the similarity of the *Lasp¹* and *Lasp^{y41}* phenotype as well as the rescue with different constructs, we continued our analysis with the *Lasp¹* allele and the L.Lasp transgene. We then tested the contractile properties of IFM with a flight assay. The flight ability of 3–5-d-old flies is partially impaired and deteriorates in older flies. Consistent with the rescue of thin filament length, flight ability is rescued by expressing L.Lasp (Fig. 1 C).

Next, we performed the same analysis in two very different muscles, the larval body wall muscle (BWM) and the tergal depressor of the trochanter (TDT), also called jump muscle. IFM is a stretch-activated muscle with fibrillar morphology, whereas TDT and BWM are muscles with tubular morphology (Schönbauer et al., 2011). Both BWM and TDT exhibit shorter sarcomere and thin filament length, as well as larval crawling and adult climbing defects, and these defects are completely rescued by reexpressing L.Lasp, except for thin filament length in BWM, which is partially rescued (Fig. S1). Thus Lasp is a general regulator of thin filament length in muscles.

I-band is wider in *Lasp¹* mutants

We next analyzed *Lasp¹* mutant IFM by EM to determine if there are additional ultrastructural defects. Longitudinal sections confirm that sarcomeres are shorter, displaying a well-arrayed sarcomeric organization regardless of their age (Fig. 2 A and Fig. S2, A and B). However, in 18-d-old *Lasp¹* mutants the I-band is wider (Fig. 2 A, compare areas marked by blue and pink arrows in close-up), and as a result the A–I junction no longer coincides with a row of electron-dense material on both sides of the Z-disc (Fig. 2 A, arrowheads). In 3-d-old flies, I-band appearance is almost wild type, suggesting that I-band stability progressively deteriorates (Fig. S2, A and B). An important role in I-band architecture is played by titin, a giant protein linking thick filaments to the Z-disc, where titin interacts with nebulin (Witt et al., 2006; Sparrow and Schöck, 2009). In *Drosophila*, the Sallimus isoform Kettin, a member of the titin family, is anchored at the Z-disc by its C terminus and extends toward the thick filaments (Bullard et al., 2006). Using immuno-EM, the Kettin KIg16 antibody has been shown to recognize an epitope located in the I-band, adjacent to the Z-disc edges (Fig. 2 B, cartoon; Burkart et al., 2007). We used structured illumination superresolution microscopy to compare Kettin localization in IFM of wild-type and *Lasp¹* mutant flies. In contrast to confocal microscopy we can now resolve two lines of Kettin, corresponding to its I-band epitope, on both sides of the Z-disc core protein α-actinin (Fig. 2 B; and compare with Fig. 1 A). Remarkably, Kettin epitopes are more widely separated in *Lasp¹* mutants compared with wild type (Fig. 2, C and D). Our data show that Kettin is improperly localized within the I-band, which may cause the observed widening of the I-band.

Moreover, the phalloidin staining also shows defects in the packing of thin filaments because individual bundles of actin filaments can be distinguished in *Lasp¹* mutant IFM (Fig. 2 C). In young *Lasp¹* mutant IFM this defect is only visible by superresolution microscopy, but in 18-d-old flies confocal microscopy is sufficient to visualize the thin filament packing defect,

indicating that thin filament stability or packing progressively deteriorates (Fig. S2 F). Thus, Lasp is also essential to stabilize actin filaments.

Lasp localizes to the Z-disc edge and the A-band

In vertebrates, nebulin extends from the Z-disc along most of the length of the thin filaments (Pappas et al., 2011). With only two nebulin repeats, Lasp cannot extend along thin filaments. We therefore asked where Lasp localizes within the sarcomere. We used full-length L.LaspGFP expressed with Mef2-Gal4 to assess Lasp localization in different muscles. Importantly, L.LaspGFP is fully functional (see Fig. 1, D and E). In BWM, L.LaspGFP colocalizes at the Z-disc with Kettin (Fig. 3 A, open arrowhead), but it also localizes at the A-band where thin and thick filaments overlap (Fig. 3 A, bracket). L.LaspGFP is excluded from the M-line in BWM. In TDT, L.LaspGFP shows a similar localization at the Z-disc and the A-band (Fig. 3 B). In IFM we can detect L.LaspGFP only at the Z-disc (Fig. 3 C, arrowhead). Lasp antibody stainings gave identical results, but with higher background (Fig. S3). We believe that Lasp is also present at the A-band region of IFM, but that L.LaspGFP cannot be properly incorporated, and the antibody cannot properly penetrate the densely packed A-band region of IFM. This is a common problem because even myosin cannot be detected at the thin–thick filament overlap zone of IFM (Fig. 3 D). In contrast, myosin can be detected at the A-band of BWM, demonstrating that the staining observed in IFM cannot be explained by the epitope recognized (Fig. 3 E). We then used superresolution microscopy to better define L.LaspGFP localization with respect to the Kettin Klg16 antibody. L.LaspGFP colocalizes with Kettin at the Z-disc periphery (Fig. 3 C). The close up of one Z-disc shows that L.LaspGFP is slightly closer to the Z-disc than the Kettin I-band epitope (Fig. 3 C, close-up). Thus, we propose that Lasp localizes at the Z-disc edges (Fig. 3 C, cartoon). Therefore, the localization of Lasp indicates that Lasp may function in two different structures, in the Z-disc and additionally at the A-band where thin and thick filaments overlap.

Lasp nebulin repeats localize and function differentially

We then asked which domain of Lasp is responsible for regulation of thin filament length. Lasp contains three distinct protein domains, a LIM domain at the N terminus followed by two nebulin repeats and an SH3 domain at the C terminus. We assayed Flag/His-tagged deletion transgenes for each domain, as well as the tyrosine to serine substitution in the actin-binding SDxxYK motif in nebulin repeat 1 (L.Lasp^{Y86S}) and nebulin repeat 2 (L.Lasp^{Y121S}; Fig. 4 A). We generated these point mutations to assess the function of each nebulin repeat independently and also because several missense mutations in human patients with NM cause a substitution of this highly conserved tyrosine (Lehtokari et al., 2006).

We first assessed the localization of the mutant Lasp proteins encoded by these transgenes with an anti-Flag antibody staining in both IFM and BWM (Fig. 4). All mutant Lasp proteins localize to the Z-disc, although L.LaspΔSH3 is weaker at
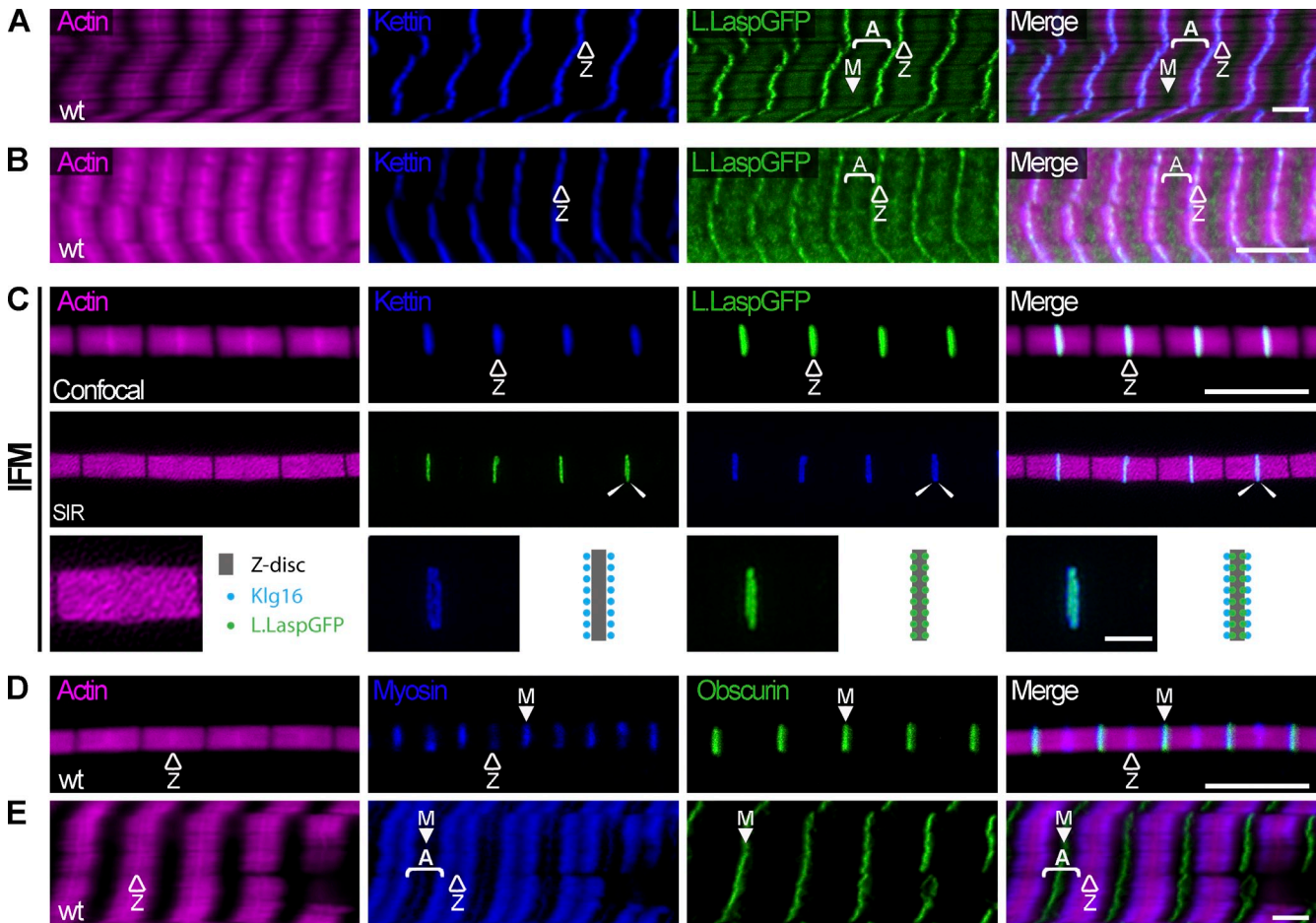
Figure 3. **Lasp localizes to the Z-disc edge and the A-band.** Wild-type muscles stained with phalloidin (magenta) to visualize thin filaments and with anti-Kettin (blue) to mark Z-discs (open arrowheads). L.LaspGFP (green) is used to observe the localization of the Lasp long isoform. (A) In BWM, L.LaspGFP localizes to both Z-disc (open arrowheads) and A-band, where thin and thick filaments overlap (bracket), but not the M-line (closed arrowheads) and I-band. (B) In TDT, L.LaspGFP localizes at the Z-disc and the A-band (bracket). (C) In IFM, L.LaspGFP colocalizes with Kettin at the Z-disc (open arrowheads). At superresolution level, L.LaspGFP partially colocalizes with Kettin antibody, with Lasp being closer to the Z-disc, which we interpret as localization at the Z-disc edge. Mef2-Gal4 driver is used to drive UAS-L.LaspGFP in a wild-type background. (D) Wild-type IFM myofibril stained with phalloidin (magenta) to visualize thin filaments, anti-myosin (blue) to visualize thick filaments, and anti-obscurin (green) to visualize the M-line. Myosin staining is only detected at the M-line and surrounding the Z-disc, not where thin and thick filaments overlap. (E) Wild-type BWM stained as in D. The zone where thin and thick filaments overlap is stained by the anti-myosin antibody. Bars: (main) 5 µm; (close-up) 1 µm. Data shown are from larvae or 3-d-old adults. SIR, structured illumination superresolution microscopy.

the Z-disc than the other Lasp proteins (Fig. 4, B and C), and L.LaspΔLIM is more spread out along the thin filaments in IFM (Fig. 4 B). L.LaspΔNEB12, L.Lasp^{Y121S}, and L.LaspΔSH3 do not localize to the A-band in BWM (Fig. 4 C). This indicates that the SH3 and LIM domains contribute to Z-disc localization, and the SH3 domain and nebulin repeats, in particular nebulin repeat 2, are required for A-band localization of Lasp. Intriguingly, we notice accumulations of Lasp and Kettin in L.Lasp^{Y121S} IFM myofibrils and bent Z-discs (Fig. 4 B, asterisk). EM confirms that these accumulations are Z-disc material (Fig. 5 A), resulting in partially and abnormally enlarged Z-discs.

We next quantified how far the mutant Lasp proteins can rescue *Lasp^{1}* IFM defects. We measured sarcomere length, thin filament length, and myofibril diameter as a readout of myofibril area (Fig. 5, C–E). We also tested adult flying ability as a physiological readout (Fig. 5 B). L.LaspΔLIM rescues thin filament length, myofibril diameter, and adult flying ability (Fig. 5, B–E). L.Lasp^{Y121S}, L.LaspΔNEB12, and L.LaspΔSH3 cannot rescue

any of the *Lasp^{1}* mutant muscle phenotypes. Sarcomere length, thin filament length, myofibril diameter, and adult flying ability are all unchanged compared with *Lasp^{1}* mutants (Fig. 5, B–E). Surprisingly, L.Lasp^{Y86S} rescues all phenotypes except myofibril diameter (Fig. 5, B–E). We observed very similar rescue results in BWM for all mutant Lasp proteins (Fig. S4), demonstrating that Lasp domains have the same function in different muscles. Therefore, these results show that the nebulin repeats and the SH3 domain are essential for Lasp localization and thin filament length determination, whereas the LIM domain of Lasp is dispensable for the parameters assayed here. Moreover, the dramatically different phenotypes of L.Lasp^{Y86S} and L.Lasp^{Y121S} demonstrate that nebulin repeats carry out distinct functions.

I-band width is set by Lasp
α-actinin interaction

To identify mechanisms of Lasp function at the I-band, we searched for Lasp-interacting partners by affinity purification and mass
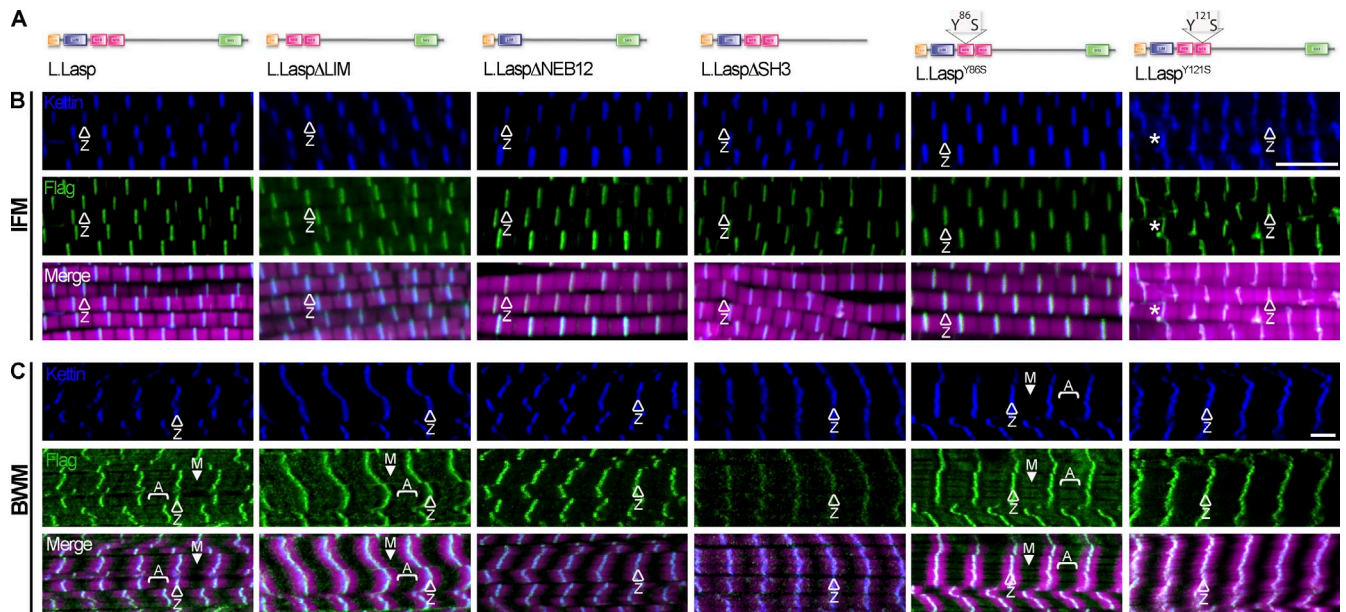
Figure 4. **Localization of mutant Lasp proteins in *Lasp¹* mutant background in IFM and BWM.** (A) Schematic representation of all Lasp proteins. Orange box, Flag/His tag; blue box, LIM domain; pink boxes, nebulin repeats; green box, SH3 domain. Localization of mutant Lasp proteins is shown in a *Lasp¹* mutant background in IFM myofibrils (B) or larval BWM (C). Z-discs are visualized by anti-Kettin antibody staining (blue), Lasp proteins with anti-Flag antibody staining (green), and thin filaments with phalloidin (magenta) in the merged image. (B) In IFM, all Lasp proteins localize to the Z-disc (open arrowheads). Deletion of the LIM domain (L.LaspΔLIM) slightly impairs localization, which appears more diffuse across the thin filaments. (C) In BWM, all Lasp proteins localize to the Z-disc (open arrowheads). The LIM domain deletion (L.LaspΔLIM) and the point mutation in the first nebulin repeat (L.Lasp^Y86S) also localize to the A-band (bracket). The nebulin domain deletion (L.LaspΔNEB12), the SH3 domain deletion (L.LaspΔSH3), and the point mutation in the second nebulin repeat (L.Lasp^Y121S) disrupt A-band localization. Moreover, the deletion of the SH3 domain leads to a weaker Z-disc localization of Lasp. Closed arrowheads indicate the M-line. Bars, 5 µm. Data shown are from larvae or 3-d-old adults.
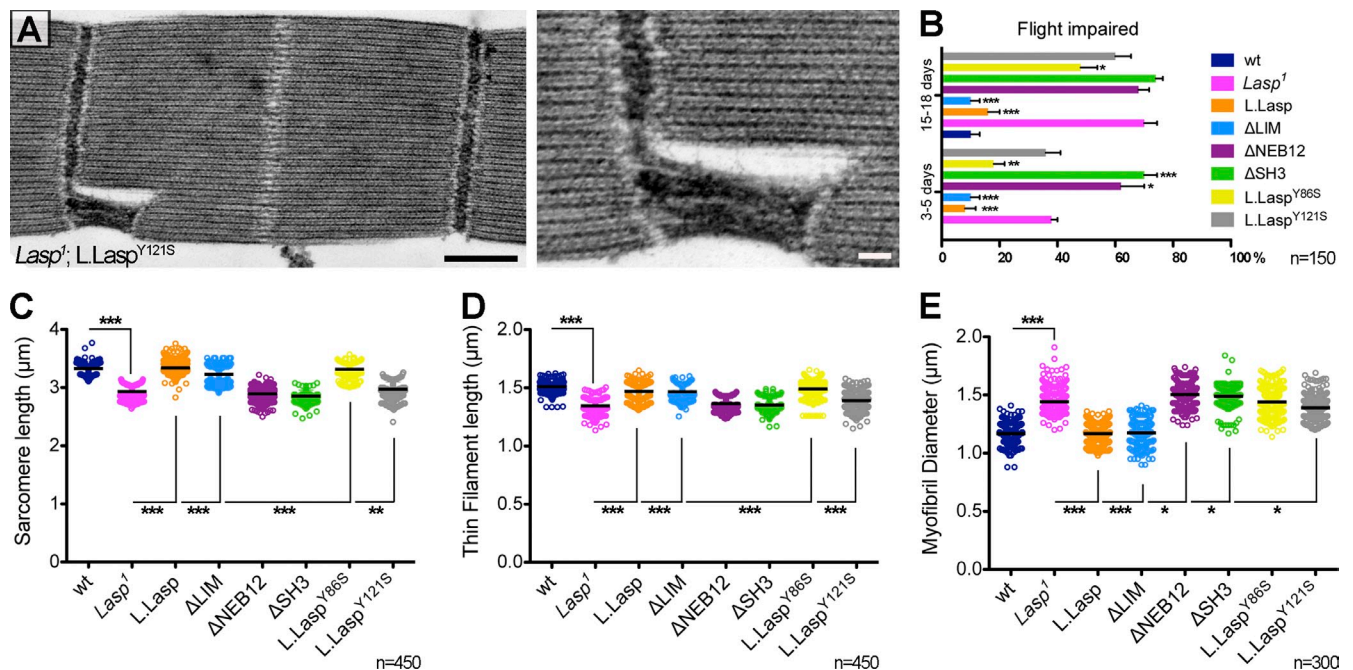

Figure 5. **Nebulin repeats have different functions.** (A) EM longitudinal section of L.Lasp^Y121S IFM myofibril showing abnormally widened Z-disc. Bars: (left) 500 nm; (right) 100 nm. (B) Rescue of flight ability of 3–5- or 15–18-d-old *Lasp¹* flies with all Lasp proteins compared with wild-type and *Lasp¹*. L.Lasp and L.LaspΔLIM fully rescue. L.LaspΔNEB12, L.LaspΔSH3, and L.Lasp^Y121S do not rescue. L.Lasp^Y86S partially rescues at 3–5 d and barely rescues at 15–18 d. The wild-type bar in 3–5-d-old flies is not visible because 0% of flies are flight impaired. Error bars indicate SD. P-values are compared with *Lasp¹*. (C–E) Sarcomere measurements from IFM of 3-d-old adults depicted as dot plot graphs showing all data points. (C) Sarcomere length. (D) Thin filament length. (E) Myofibril diameter. L.Lasp fully rescues all parameters assayed. L.LaspΔLIM rescues fully except for sarcomere length. L.LaspΔNEB12, L.LaspΔSH3, and L.Lasp^Y121S do not rescue any of the phenotypes. L.Lasp^Y86S rescues sarcomere and thin filament length, but not myofibril diameter. ***, P < 0.0001; **, P < 0.001; *, P < 0.01; no p-value indicates no significant difference to *Lasp¹*. *n* refers to sarcomeres measured or flies tested for each genotype.
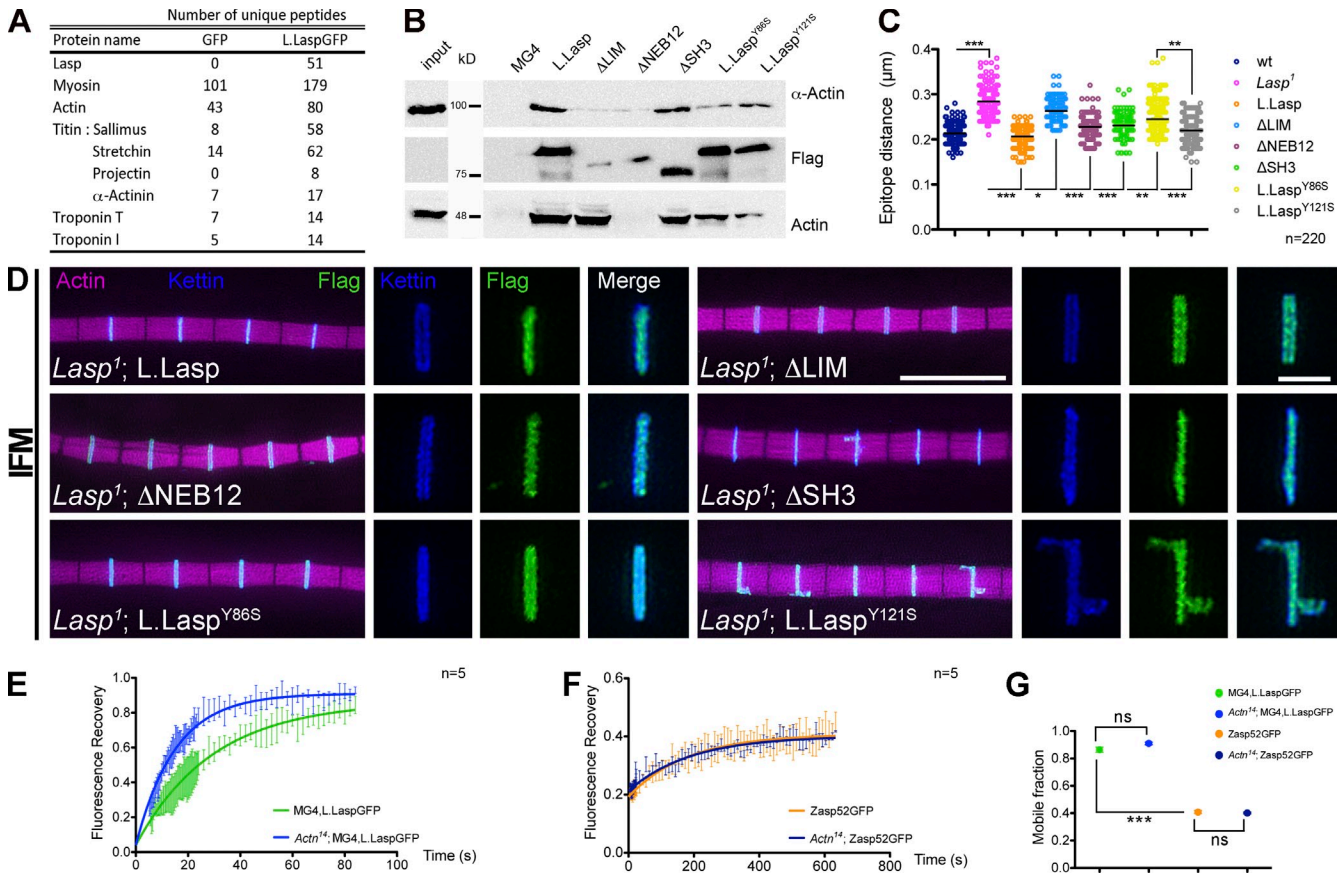
Figure 6. Lasp α-actinin interaction stabilizes I-band width. (A) Summary of mass spectrometry results. L.LaspGFP was affinity purified from IFM extracts with GFP antibody–coupled beads. Numbers indicate unique peptides from Mef2-Gal4 UAS-L.LaspGFP and twi-Gal4 UAS-2xGFP control pull-down. (B) Two-step affinity purification using Flag- and His-tagged L.Lasp followed by Western blotting confirms that L.Lasp interacts with α-actinin and actin. Mef2-Gal4 (MG4) was used as a control and shows no interaction. Nebulin repeats are required for interaction with actin, whereas both nebulin repeats and the LIM domain of Lasp is required for interaction with α-actinin. (C) Quantification of distance between Kettin Klg16 epitopes in rescue assays with all Lasp proteins. ***, $P < 0.0001$; **, $P < 0.001$; *, $P < 0.01$. L.Lasp^{Y121S} distances were determined at normal areas, not abnormally widened Z-discs. (D) Superresolution imaging of anti-Kettin (blue) and actin staining (magenta) of all Lasp proteins (anti-Flag in green). L.Lasp^{Y121S}, L.LaspΔSH3, and L.LaspΔNEB12 show actin packing or stability defects. In L.Lasp^{Y86S} and L.LaspΔLIM, Lasp is widely spaced, colocalizing with Kettin. In L.LaspΔSH3, Lasp localizes in a narrow line at the Z-disc. Bars: (main) 5 μm; (close-up) 1 μm. (E) FRAP recovery curve of L.LaspGFP in wild type versus Actn^{14} mutant. L.LaspGFP exchange is faster in Actn^{14} than in wild type. (F) FRAP recovery curve of Zasp52GFP in wild type versus Actn^{14} mutant. Zasp52GFP recovers slowly compared with LaspGFP, and its dynamics do not change in the Actn^{14} mutant. Values are means ± SEM. (G) Mobile fraction of L.LaspGFP versus Zasp52GFP in wild type versus Actn^{14} mutant. The Zasp52GFP control is considerably less mobile. ***, $P < 0.0001$; ns, not significant. Data shown are from larvae or 3-d-old adults.

spectrometry. We expressed a GFP-tagged L.Lasp transgene in muscles and affinity-purified L.LaspGFP protein from a total protein extract of dissected thoraces. As a control, we purified GFP alone from the same tissue. We identified five groups of proteins by mass spectrometry, which associate with L.Lasp protein: three different titin family members (Sallimus, Projectin, and Stretchin), α-actinin, troponins, actin, and myosin (Fig. 6 A). In vertebrates the interaction of nebulin with titin is already well described. In vitro studies indicate that these two giant proteins interact at the Z-disc edge (Witt et al., 2006). The mass spectrometry data combined with the I-band phenotype suggest the same interaction occurs in *Drosophila*. We therefore first focused on the interaction of Lasp with α-actinin to uncover a possible mechanism for the I-band defect. To confirm the mass spectrometry data, we performed an independent pull-down assay, with transgenes expressing Flag/His double-tagged Lasp proteins, first over Flag beads, then over nickel beads, followed by immunoblotting. Full-length L.Lasp interacts specifically with

α-actinin (Fig. 6 B). Moreover, pull-downs with mutant Lasp proteins show that α-actinin interacts with the LIM domain and the nebulin repeats, possibly interacting more strongly with nebulin repeat 1 than nebulin repeat 2 (Fig. 6 B). The direct interaction of Lasp with actin was already demonstrated in vitro (Suyama et al., 2009). Our interaction data extend these results by showing that Lasp interacts with actin through the nebulin repeats and, surprisingly, interacts more efficiently with nebulin repeat 2 than nebulin repeat 1 (Fig. 6 B).

Given that Kettin localization is altered in *Lasp^1* mutants (Fig. 2 D), we first asked how Kettin localization correlates with the protein interactions we observed. We therefore measured the distance between Kettin epitopes in our rescue assay with all mutant Lasp proteins (Fig. 6 C). L.Lasp rescues Kettin epitope spacing (Fig. 6 C). In the absence of the LIM domain, Kettin epitopes as well as Lasp itself are spaced further apart (Fig. 6, C and D), which correlates with the requirement of the LIM domain for interaction with α-actinin (Fig. 6 B). Rescue is more

intermediate for the other transgenes, but two observations are noteworthy: L.Lasp^{Y121S}, which interacts more strongly with α-actinin, rescues the Kettin epitope distance significantly better than L.Lasp^{Y86S} (Fig. 6, C and D); and L.LaspΔSH3 protein collapses into a narrow stripe at the center of the Z-disc (Fig. 6 D). These data indicate that the Lasp α-actinin interaction modulates Kettin localization within the I-band.

Finally, the phalloidin staining shows that L.LaspΔNEB12, L.Lasp^{Y121S}, and L.LaspΔSH3 incompletely rescue actin thin filament defects, with L.LaspΔNEB12 being least able to rescue (Fig. 6 D).

To further clarify the importance of the interaction with α-actinin, we performed a FRAP assay in third instar larvae with L.LaspGFP (Fig. 6, E–G; and Fig. S5 C). We compared Lasp dynamics in wild-type larvae with *α-actinin* null mutant larvae (*Actn^{14}*). *Actn^{14}* larvae entirely lack α-actinin (Fig. S5, A and B). By confocal microscopy, L.LaspGFP still localizes at the Z-disc in *Actn^{14}* larvae, indicating that α-actinin cannot be the only protein recruiting Lasp to the Z-disc (Fig. S5 A). As indicated by the steeper slope, the recovery rate of L.LaspGFP is faster in *Actn^{14}* mutants than in wild type (Fig. 6 E). We recently demonstrated that Zasp52, a core protein of the Z-disc, interacts directly with α-actinin and is required for Z-disc assembly (Katzemich et al., 2013). The recovery rate of Zasp52GFP is slower than of LaspGFP, but identical in wild-type and *Actn^{14}* larvae, demonstrating that Zasp52 dynamics are not affected by the absence of α-actinin (Fig. 6 F). Moreover, Lasp is much more mobile compared with Zasp52 (Fig. 6 G). These data indicate that Lasp is a peripheral Z-disc protein, in part recruited by α-actinin.

Myosin interaction may set filament spacing at the A-band

The increased myofibril diameter of *Lasp^1* mutant IFM (Fig. 5 E) suggests a larger cross-sectional area of IFM myofibrils. Furthermore, the A-band localization of Lasp in BWM and TDT suggests additional defects at the A-band, where thin and thick filaments overlap. We therefore performed EM cross sections of IFM at the A-band level. These cross sections reveal that *Lasp^1* mutant myofibrils are indeed larger than the wild type because of two separate defects: a 50% increase in the number of filaments and an increase in filament spacing (Fig. 7, A and B). Filament spacing is illustrated in the cross section close-up by comparing the blue and pink hexagon (Fig. 7 A). These defects could be a compensation for shorter thin filament length to alleviate the deteriorating flight ability of older flies. However, both of these defects are identical in young and old flies (Fig. S2, C–E), indicating that they are independent phenotypes.

We next asked if A-band localization correlates with proper filament spacing and filament number. We chose to analyze our point mutations L.Lasp^{Y86S} and L.Lasp^{Y121S} because they minimally disrupt full-length Lasp yet show differential localization at the A-band in BWM (see Fig. 4 C). L.Lasp^{Y86S}, which localizes normally at the A-band in BWM, partially rescues IFM filament spacing but not filament number. In contrast, L.Lasp^{Y121S}, which does not localize at the A-band in BWM, cannot rescue IFM filament spacing but partially rescues filament number (Fig. 7,

A and B). Thus, nebulin repeat 1 is more involved in setting filament number, whereas nebulin repeat 2 predominantly mediates filament spacing. In addition, L.Lasp^{Y121S} exhibits misalignment of thin filaments (Fig. 7 A, close-up). Our affinity purification and mass spectrometry revealed myosin as a good candidate for interaction with Lasp because of a peptide difference between control and experiment similar to Lasp itself (Fig. 6 A). To further assess this potential interaction, we used an independent transgene encoding double-tagged Lasp and performed a two-step affinity purification over Flag beads and nickel beads. This shows that L.Lasp efficiently coimmunoprecipitates myosin, whereas Mef2-Gal4 control flies barely do (Fig. 6 C). We then determined if association with myosin is reduced in L.Lasp^{Y121S} mutants, which could explain the inability to localize at the A-band. Our pull-down assays show that mutant Lasp proteins not localizing at the A-band, namely L.Lasp^{Y121S}, L.LaspΔNEB12, and L.LaspΔSH3, can interact with myosin only at background levels, whereas L.LaspΔLIM and L.Lasp^{Y86S} interact well with myosin (Fig. 7 C). This suggests that Lasp interaction with both actin and myosin mediates the filament spacing defect. To further characterize the interaction of Lasp with myosin, we isolated thick filaments from IFM of *Act88F^{KM88}* mutant flies. *Act88F^{KM88}* flies entirely lack thin filaments in IFM (Beall et al., 1989). This is confirmed by Western blotting of IFM extracts, which have only negligible amounts of actin (Fig. 7 E). Bacterially purified recombinant L.Lasp cosediments with thick filaments, suggesting that L.Lasp likely interacts directly with myosin thick filaments (Fig. 7 D).

Discussion

By analyzing *Drosophila* Lasp, we can show that a nebulin family member with only two nebulin repeats is sufficient to regulate thin filament length. In addition, Lasp localization and biochemical interactions indicate that Lasp uses different protein domains to mediate filament spacing at the A-band versus I-band architecture and maintenance at the Z-disc edge.

Lasp or its orthologues is one of the few muscle proteins conserved in all Eumetazoans and therefore in all organisms with striated muscles (Steinmetz et al., 2012). This indicates that nebulin repeats play an ancient and conserved role in modulating muscle function. This notion is supported by the *Lasp^1* mutant phenotype, which exhibits several similarities with vertebrate *nebulin* mutants, in particular the partial widening of Z-discs (Fig. 5 A) and shorter sarcomere and thin filament length leading to impaired muscle function (Figs. 1 and S1).

As Lasp does not coalign with thin filaments across the I-band (Fig. 3), neither the nebulin ruler nor the two-segment model (Gokhin and Fowler, 2013) can explain thin filament length regulation in *Drosophila*. However, our data show that Lasp stabilizes actin filaments in agreement with what has been reported for nebulin (Pappas et al., 2010). In contrast to superresolution or confocal analysis (Figs. 2 C and S2 F), ultrastructural analysis of *Lasp^1* mutant myofibrils revealed no apparent thin filament defect in the longitudinal sections regardless of their age (Fig. 2 A and Fig. S2, A and B). This is likely explained by different dissection procedures. For EM imaging, half thoraces
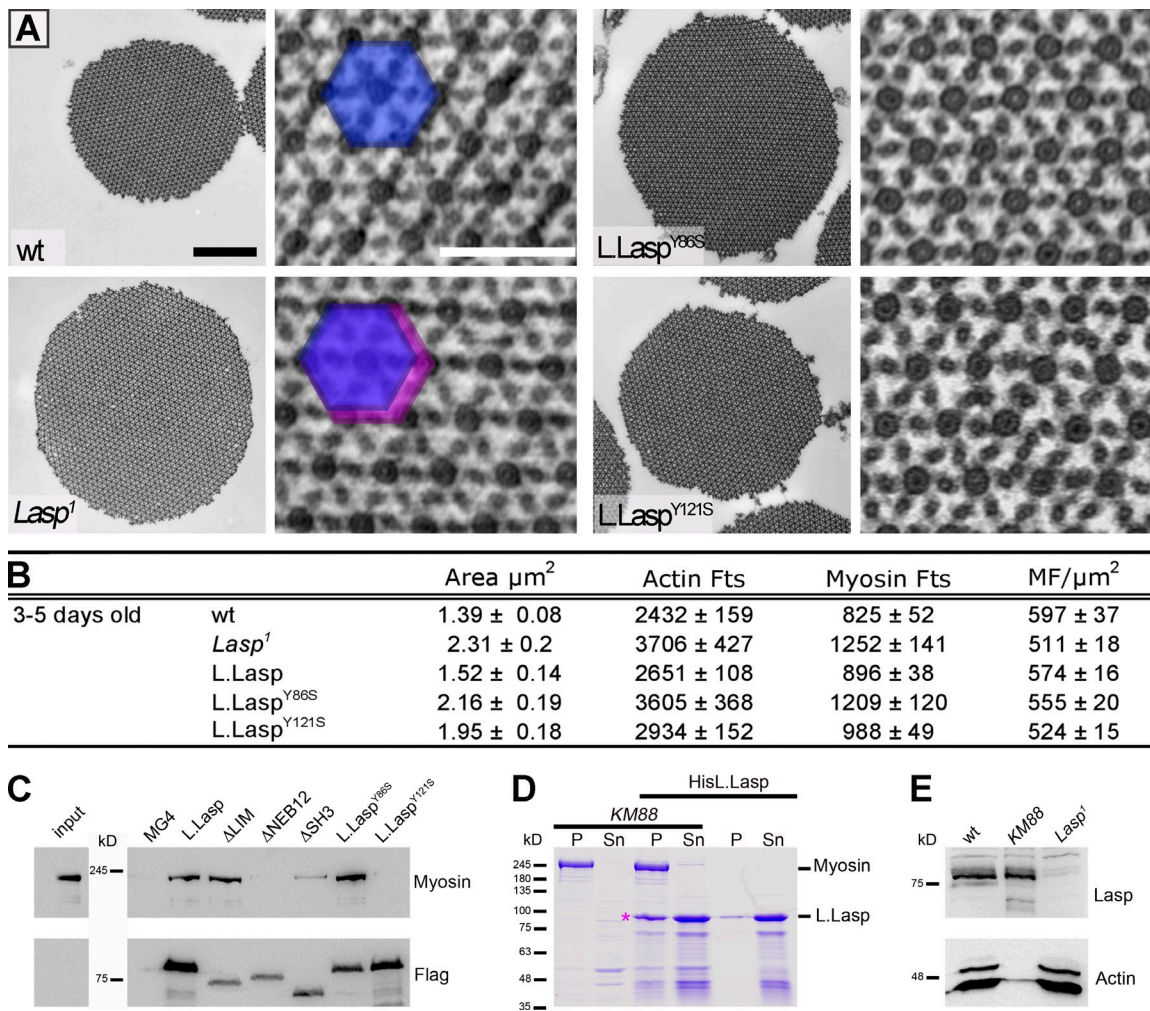
Figure 7. **Lasp mediates filament spacing.** (A) EM cross sections of 3–5-d-old IFM myofibrils reveal that *Lasp¹* myofibrils are larger and filaments more widely spaced (compare blue and pink hexagon). In addition, actin thin filaments are improperly arranged in L.Lasp^{Y121S}. Bars: (main) 500 nm; (close-up) 100 nm. (B) Quantification of cross-sectional area, actin and myosin filaments (Fts) per myofibril, and myosin filament (MF) density. For different reasons, neither L.Lasp^{Y86S} nor L.Lasp^{Y121S} properly rescues cross-sectional area. L.Lasp^{Y86S} partially rescues filament spacing, but not filament number, whereas L.Lasp^{Y121S} partially rescues filament number, but not filament spacing. $n = 10$ myofibrils from five different flies. (C) Pull-down assay with different Lasp proteins shows that L.Lasp, L.LaspΔLIM, and L.Lasp^{Y86S} interact with myosin, whereas L.LaspΔNEB12, L.LaspΔSH3, and L.Lasp^{Y121S} interact with myosin only at background levels. Mef2-Gal4 (MG4) was used as control. (D) Cosedimentation assay of HisL.Lasp with myosin thick filaments. *Act88F^{KM88}* mutant IFM extracts consisting mostly of thick filaments were incubated for 1 h with or without bacterially purified HisL.Lasp (10 µM) and then pelleted by ultracentrifugation. Pellet (P) and supernatant (Sn) are equally loaded on an 8% SDS-PAGE gel, which was stained with Coomassie. HisL.Lasp cosediments with thick filaments (asterisk). (E) Western blot of IFM extracts indicate almost complete absence of actin in *Act88F^{KM88}* IFM extracts.

are fixed before embedding and then ultrathin sections are cut deep in the muscle fibers; in contrast, for superresolution and confocal microscopy, myofibers are manually extracted from IFM and separated into single myofibrils by pipetting up and down. The mechanical stress is the only relevant difference between the two protocols indicating that actin filaments are less stable in *Lasp¹* mutant myofibrils. This is further supported by the ability of L.Lasp to rescue the misalignment of thin filaments, whereas L.LaspΔNEB12, which is unable to bind actin, is least able to rescue thin filament defects (Fig. 6, B and D). Our combined data do not suggest a unique mechanism of thin filament length regulation, but rather a general stabilization of actin filaments by binding of nebulin repeats to thin filaments at the Z-disc and the A-band.

Structural studies on nebulin-deficient mice showed that in the absence of nebulin, Z-discs occasionally widen, especially in older mice, and myofibrils are misaligned (Bang et al., 2006; Witt et al., 2006; Tonino et al., 2010). Similar defects are observed in biopsies from human patients (Ottenheijm et al., 2009). Thus, the functional roles of nebulin extend beyond thin filament length regulation. Similarly, we observe the occasional breakdown of Z-disc width regulation in L.Lasp^{Y121S} mutants, which show abnormally widened Z-discs, usually at the periphery of myofibrils (Fig. 5 A). In vertebrates, titin and nebulin interact at the Z-disc edge, and this interaction is believed to specify Z-disc width (Witt et al., 2006). We propose that at the Z-disc edge Lasp links the Z-disc core protein α-actinin with thin filaments and anchors the Sallimus isoform Kettin. Sallimus forms an elastic link between the Z-discs and the ends of thick filaments similar to titin in vertebrates (Bullard et al., 2006). Our affinity purification and mass spectrometry analysis uncovered all three proteins: α-actinin, actin, and Sallimus (Fig. 6 A).

Moreover, coimmunoprecipitation experiments with mutant Lasp proteins confirm the interaction with actin and α-actinin (Fig. 6 B). α-Actinin interacts with the LIM domain and nebulin repeats of Lasp (Fig. 6 B). In vertebrates, in vitro studies have demonstrated that the nebulin family member N-RAP also interacts with α-actinin through its LIM domain and nebulin repeats, indicating that this interaction may be conserved across evolution (Lu et al., 2003). Finally, the FRAP assay indicates that Lasp is in part tethered to the Z-disc by α-actinin (Fig. 6 E). Our mutant phenotype and the rescue and localization data also support a link of Lasp with Kettin, even though the biochemical interaction of these proteins remains to be tested. First, Lasp localizes at the Z-disc edges (Fig. 3 C). Second, in $Lasp^1$ mutant IFM, superresolution microscopy shows a wider spacing of Kettin I-band epitopes (Fig. 2 C), likely leading to a wider I-band as observed by EM (Fig. 2 A). Most importantly, when Lasp can no longer interact with α-actinin (Fig. 6, B and D, L.LaspΔLIM), Lasp signal is more widely spaced and colocalizes perfectly with the Kettin I-band epitope. In contrast, Lasp collapses into a single line at the Z-disc core, when the SH3 domain is deleted, which at least in vertebrate nebulin is required for interaction with titin (Witt et al., 2006; Fig. 6 D, L.LaspΔSH3). We therefore propose that Lasp ensures proper insertion of Kettin into the Z-disc. Deterioration of I-band integrity over time also indicates that Lasp plays a role in maintaining I-band structure during muscle contraction. In addition, actin binding of Lasp must also be important for I-band integrity because regulation of Z-disc width can break down completely in L.Lasp^{Y121S}, which interacts weakly with actin (Fig. 5 A and Fig. 6 B). Because L.LaspΔLIM fully rescues thin filament length (Fig. 5 D), interactions resulting in I-band defects play no role in setting thin filament length.

In addition to the Z-disc edges, Lasp also localizes to the A-band in TDT and BWM. The filament-packing defects, the myosin interactions, and the differential localization of nebulin repeat mutations L.Lasp^{Y86S} and L.Lasp^{Y121S} all support the hypothesis that nebulin repeat 2 specifically interacts with myosin thick filaments, thereby affecting filament spacing at the A-band (Fig. 4 C and Fig. 7, A–C). Furthermore, bacterially purified Lasp cosediments with thick filaments isolated from IFM of $Act88F^{KM88}$ mutant flies, which lack actin thin filaments in the IFM (Fig. 7 D). EM of $Act88F^{KM88}$ mutant IFM shows thick filaments organized around rudimentary M-lines, but no evidence of any thin filaments or Z-disc structures (Beall et al., 1989). This indicates that the interaction of Lasp with myosin thick filaments does not occur indirectly through actin.

We also observed shorter myosin thick filaments in $Lasp^1$ mutants (Fig. 2 A, Fig. 5 A, and not depicted). In invertebrates, thick filament length varies considerably both between muscle types (Fig. 3, compare E and D) and during development of individual muscles, for example, IFM, where thick filament length increases during pupariation (Reedy and Beall, 1993). The observed change in thick filament length is therefore likely an adaptation to shorter thin filament length; however, a more direct effect on thick filament stability similar to Flightin cannot be excluded (Reedy et al., 2000).

Importantly, our data demonstrate that nebulin repeats carry out distinct functions: nebulin repeat 2 binds myosin, interacts more strongly with actin, and mediates A-band localization and filament spacing (Fig. 4 and Fig. 7, A–C). In contrast, nebulin repeat 1 interacts better with α-actinin (Fig. 6 B) and plays a bigger role in setting filament number than nebulin repeat 2 (Fig. 7, A and B). The nebulin repeat 1 mutation, L.Lasp^{Y86S}, may also participate in filament spacing, as it does not fully rescue filament spacing (Fig. 7 B). A better biochemical characterization should clarify these differences in the future. Intriguingly, L.Lasp^{Y86S} completely rescues thin filament length, yet older flies are flight impaired, suggesting that changes in filament number or spacing contribute substantially to power output. Finally, only the mutation in nebulin repeat 2 causes an abnormal widening of Z-discs, suggesting it plays a role in Z-disc termination, perhaps related to its impaired interaction with actin. We propose that vertebrate nebulin fulfills these different functions with different nebulin repeats of the same molecule. This is supported by biochemical data showing that N-terminal nebulin repeats situated in the A-band, but not C-terminal nebulin repeats, interact with myosin and regulate actomyosin ATPase activity (Root and Wang, 1994). Therefore mutations in different subsets of human nebulin repeats may give rise to different NM phenotypes.

We propose the following mechanisms for Lasp function at the A-band and the Z-disc (Fig. 8). At the A-band, Lasp nebulin repeat 2 may simultaneously interact with thin and thick filaments to regulate proper filament spacing. This likely fine-tunes proper power output because changes in filament spacing are known to affect power output in IFM (Tanner et al., 2012; Fig. 8 A′). At the Z-disc, all domains of Lasp may simultaneously interact with α-actinin, actin, and the titin family member Kettin, and these interactions ensure proper insertion of titin-like molecules at the Z-disc and thereby stabilize the entire I-band (Fig. 8 A″). In addition to the LIM domain, Lasp nebulin repeats also interact with α-actinin (Fig. 6 B), and especially nebulin repeat 1 contributes to I-band architecture (Fig. 6 C). Finally, Lasp likely also specifies the number of filaments incorporated into each myofibril through nebulin repeat 1 (Fig. 7, A and B).

As vertebrate nebulin does not have a LIM domain, the LIM domain–dependent I-band function of Lasp could be taken over by vertebrate N-RAP or Lasp-2, which contains an N-terminal LIM domain.

Because of the small size of Lasp compared with nebulin and its distinct localization, Lasp is a suitable model system to gain further insights into the in vivo function of nebulin repeats in normal physiology and disease.

Materials and methods

Fly stocks and genetics
UAS-L.Lasp (amino acids 1–657 corresponding to Lasp-PB in FlyBase), UAS-S.Lasp (amino acids 1–504 corresponding to Lasp-PA in FlyBase), UAS-L.LaspGFP, UAS-L.LaspΔLIM (deletion from T4 to H100), UAS-L.LaspΔNEB (deletion from A106 to K171), UAS-L.LaspΔSH3 (stop at D507), UAS-L.Lasp^{Y86S}, and UAS-L.Lasp^{Y121S} transgenic lines were generated by P-element transformation. The following stocks were used (see FlyBase for complete description): ry^{506} $Act88F^{KM88}e^s$ (provided by A. Cammarato,
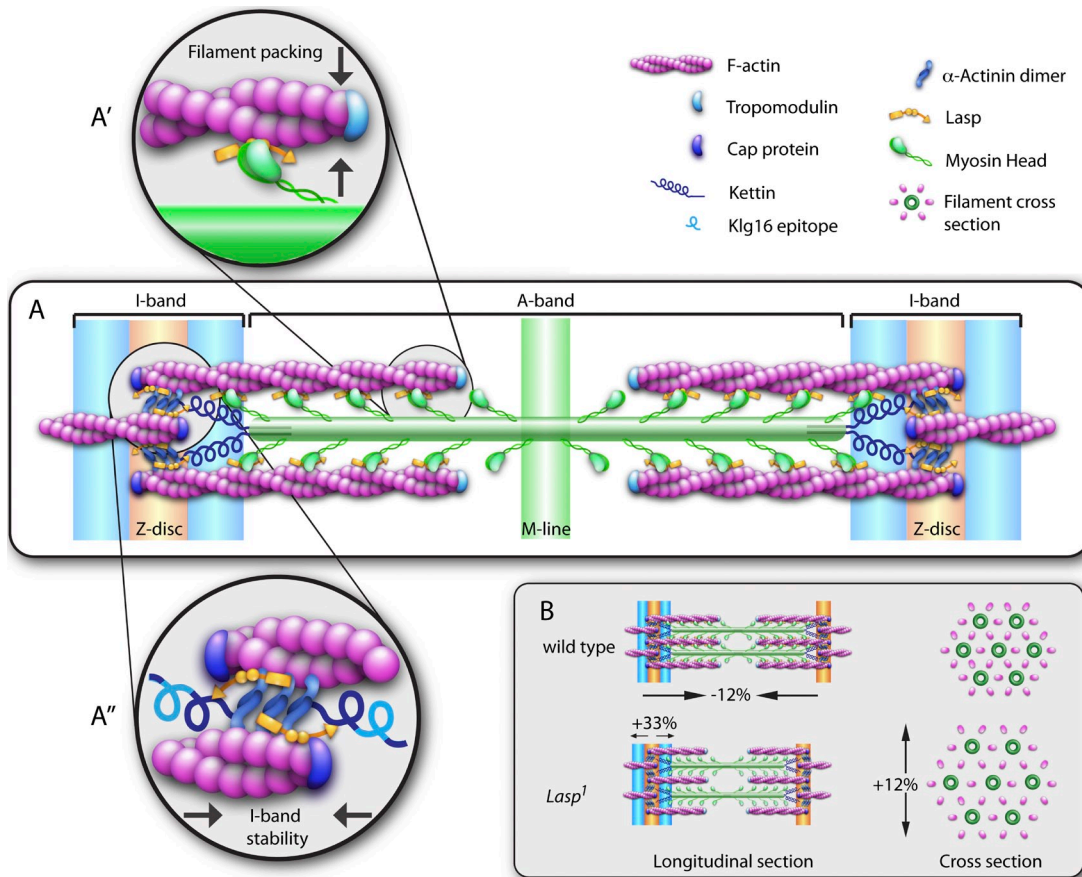
Figure 8. Model of Lasp function. (A) The arrangement of thick myosin and thin actin filaments in the relaxed state. A Kettin molecule is attached to the Z-disc and spans the distance to the end of a thick filament. Thick filaments are thus connected at both ends to Z-discs through Kettin. At the I-band the Kettin molecule is elastic and changes length as the sarcomere contracts and relaxes. Thin filaments are anchored at the Z-disc by the cross-linking protein α-actinin and are capped at both ends. Tropomodulin caps the pointed end of thin filaments. Capping protein caps the barbed end at the Z-disc. (A′) Lasp may interact simultaneously with thin and thick filaments to maintain proper filament spacing at the A-band. (A″) At the Z-disc, Lasp is associated with thin filaments through its nebulin repeats and also binds directly or indirectly to α-actinin and Kettin. α-Actinin binding of Lasp may properly tether Kettin to the Z-disc, which is necessary for I-band stability. (B) In a wild-type sarcomere Lasp maintains I-band width and proper filament spacing and number and thereby also stabilizes thin filament length. In a *Lasp[1]* mutant sarcomere, I-bands are wider and filament spacing and number of filaments per sarcomere (not depicted) are increased, whereas thin filament length is decreased. The precise orientation and number of Lasp molecules with respect to other sarcomeric proteins in these cartoons is hypothetical.

Johns Hopkins University School of Medicine, Baltimore, MD), *Lasp[1]* (Lee et al., 2008), *Lasp[Y41]* (provided by A. Ephrussi, European Molecular Biology Laboratory, Heidelberg, Germany; Suyama et al., 2009), and Mef2-Gal4, G00189 (GFP-Zasp52), and *Actn[14]* from the Bloomington Drosophila Stock Center.

The following recombinants and stocks were generated by standard genetic crosses: *Lasp[1]* UAS-L.LaspGFP, *Lasp[1]* UAS-L.Lasp, *Lasp[1]* UAS-S.Lasp, *Lasp[1]* UAS-L.LaspΔLIM, *Lasp[1]* UAS-L.LaspΔNEB12, *Lasp[1]* UAS-L.LaspΔSH3, *Lasp[1]* UAS-L.Lasp[Y86S], *Lasp[1]* UAS-L.Lasp[Y121S], *Lasp[1]* Mef2-Gal4, Mef2-Gal4 UAS-L.Lasp, Mef2-Gal4 UAS-L.LaspGFP, Mef2-Gal4 UAS-L.LaspΔLIM, Mef2-Gal4 UAS-L.LaspΔNEB12, Mef2-Gal4 UAS-L.LaspΔSH3, Mef2-Gal4 UAS-L.Lasp[Y86S], and Mef2-Gal4 UAS-L.Lasp[Y121S]. Lines were kept over balancer chromosomes carrying twist-Gal4 UAS-2xGFP.

Molecular procedures and antibody production

All Lasp constructs were synthesized by GenScript or generated by standard cloning procedures. Each construct was then cloned into pP{UASt} (see FlyBase for complete description). For protein production for the cosedimentation assay, L.Lasp was cloned into pRSET-A (Life Technologies) and transformed into *Escherichia coli* strain BL21. For antibody production, S.Lasp cDNA from Expressed Sequence Tag AT23571 was cloned into pBAD-DEST49 (Life Technologies), expressed, purified, and used for immunization of rats and rabbits according to standard procedures (Cell Imaging and Analysis Network, McGill University). All constructs were verified by sequencing.

Behavioral assays

For the crawling assay, third instar mutant larvae were identified by the absence of the GFP balancer. Five larvae of the desired genotype were placed on a 5-cm fresh apple juice plate marked with zones of five concentric circles (Fig. S1 D) and zonal location of each larva was recorded after 60 s. These measurements were performed in triplicate for each group of five, and data for 12 independent sets (60 animals coming from three different crosses) were collected.

Flight and climbing assays were performed with 3- to 5-d-old or 15- to 18-d-old flies at RT. For flight tests, flies were released in sets of 10 animals from the center of a flight chamber. Light was placed at the top of the flight chamber to attract flies and only flies flying up were considered to be able to fly. For climbing assays, 10 adult flies were transferred to an empty vial and lightly tapped to the bottom. The number of flies that climbed to a height of 7 cm within 10 s was recorded. Data for five independent sets of 10 flies (50 animals coming from three different crosses) were collected for both assays. In all assays, Mef2-Gal4 flies were used as wild-type controls.

The relative distribution of animals at the end of the motility, flight, or climbing assay was plotted in GraphPad Prism (GraphPad Software), using the mean percentage of animals present in each zone or not flying or climbing.

Immunostainings

We used the following primary antibodies for immunofluorescent stainings of IFMs: rat anti–α-actinin MAC276, rat anti-Kettin Klg16 MAC155,

and rat anti-myosin MAC147 at 1:200 (Babraham Bioscience Technologies); rabbit anti-Obscurin Kin1 at 1:200 (provided by B. Bullard, University of York, York, UK; Katzemich et al., 2012); mouse anti-Flag at 1:600 (Sigma-Aldrich); rabbit anti–Lasp-C at 1:2,000 (provided by A. Ephrussi; Suyama et al., 2009); and rabbit anti–S-Lasp at 1:1,000. Phalloidin-TRITC (Sigma-Aldrich) or phalloidin–Alexa Fluor 647 (Life Technologies) was used to label F-actin.

IFM and TDT were prepared and stained as described previously (Katzemich et al., 2013). In brief, half thoraces were glycerinated (20 mM sodium phosphate, pH 7.2, 2 mM MgCl$_2$, 2 mM EGTA, 5 mM DTT, 0.5% Triton X-100, and 50% glycerol) overnight at −20°C. IFMs or TDTs were dissected, washed in relaxing solution (20 mM sodium phosphate, pH 7.2, 5 mM MgCl$_2$, 5 mM ATP, and 5 mM EGTA) with protease inhibitors, and separated into single myofibrils by pipetting or left as a whole. Primary antibody incubation was performed overnight, followed by washes in relaxing solution and 2-h incubations of secondary antibodies (Alexa Fluor series; Life Technologies) and phalloidin.

For BWM, larvae were dissected on silgard plates in relaxing solution and then fixed in 4% paraformaldehyde in relaxing solution. Larval fillets were rinsed in PBS, incubated in PBT (PBS plus 0.3% Triton X-100) at RT for 15 min, and followed by 1-h incubation at RT in PBT-BSA (PBT plus 1% BSA). Primary antibody incubation was performed overnight, followed by washes in PBT-BSA and 2-h incubation with secondary antibodies. After washes in PBT, fillets were incubated in PBT plus phalloidin at RT for 20 min and finally rinsed in PBT.

Samples were mounted in ProLong Gold antifade solution (Life Technologies). Laser scanning confocal images were acquired at RT on a microscope (LSM 510 Meta; Carl Zeiss) using a 63×, 1.4 NA Plan Apochromat oil immersion objective with the confocal-associated acquisition software (Carl Zeiss). Superresolution images were acquired at RT on a V4 Blaze OMX system (GE Healthcare) with an Evolve EM-CCD camera using a 100×, 1.4 NA U-PLANAPO oil immersion objective (Olympus). Images were processed with SoftWoRx software (GE Healthcare) using structured illumination reconstruction and image registration to reconstruct the image and correct for chromatic aberrations and camera misalignment. Then, images were flattened by maximum intensity projection (ImageJ).

Statistical analyses on length measurements
For rescue assays, three independent crosses were performed and rescued animals were selected by the absence of the GFP balancer. For BWM, at least 10 fillets were dissected and stained for each cross (30 larvae in total/genotype) and at least one image of the VL3 muscle was acquired per fillet. For adult myofibrils, IFM or TDT, at least 10 thoraces were dissected and stained for each cross (30 flies in total/genotype) and at least 10 images were acquired for each preparation. 30 to 40 images were analyzed with ImageJ measurement tools: a line was drawn from Z-disc to Z-disc (anti-Kettin staining) to measure sarcomere size or across the Z-disc from thin filament pointed end to pointed end (phalloidin staining) and then divided by two to obtain thin filament length. For Kettin epitope distance, 10 thoraces were dissected and stained from two independent crosses (20 flies in total/genotype) and at least 10 images were acquired for each. Then, data were transferred for further analyses to GraphPad Prism. Dot plot graphs represent all the measurements done and their distribution around the average (450 measurements for IFM, 150 measurements for TDT, 430 measurements for BWM, and 220 measurements for Kettin epitope distance). Student's t test was used to determine if two sets of data were significantly different from each other. In all assays, Mef2-Gal4 flies were used as wild-type controls.

FRAP analysis
Heterozygous mutant females for α-actinin (Actn^{14}/FM7a) were crossed to the recombinant line Mef2-Gal4, UAS-L.LaspGFP. Eggs were collected for 4 h on an apple juice plate and aged for 3 d at 25°C. Male third instar larvae, carrying the Actn^{14} mutation and expressing L.LaspGFP, were selected and anesthetized for 15 min in Kwan Loong Medicated Oil (25% menthol, 15% methyl salicylate, 10% camphor, 10% eucalyptus oil, 7% lavender oil, and 0.5% chloroform). Larvae were then mounted in between two spacers on double-sided tape and covered with mineral oil. Heart beating was verified before acquisition to ensure larvae were alive during the recording. Fluorescence recovery was recorded for 3 (L.LaspGFP) or 10 min (Zasp52GFP) with a 491-nm laser at low power, imaging every 2 or 10 s. Three larvae from three different crosses (at least nine different animals for each genotype) were analyzed and five independent recordings were done for each. Data were analyzed using ImageJ software. Gray intensities for bleached Z-disc, unbleached Z-disc, and background

region were determined manually for each image in a time series. Normalized intensity was obtained using the following equation: $I_{Norm} = (I_{bleach} − I_{background})/(I_{nonbleach} − I_{background})$.

Finally, five independent recovery normalized datasets (bleaching not below 80%) were averaged using GraphPad Prism software. The fitted curve as well as the mobile fraction was calculated by the software. Images were acquired at RT with Metamorph software (Molecular Devices) on a Quorum WaveFX spinning disk confocal system with an EM-CCD camera (Hamamatsu) on an inverted microscope (DMI6000B; Leica) using a 63×, 1.40–0.6 HCX Plan Apochromat oil immersion objective.

Immunoprecipitation and binding assays
For the affinity purification, 200 adult fly thoraces expressing UAS-L.Lasp-GFP with Mef2-Gal4 were cut in half and incubated overnight in lysis buffer (50 mM Tris-HCl, pH 8, 1 M NaCl, 1 mM EDTA, 0.5% Triton X-100, and complete EDTA-free protease inhibitor cocktail [Roche]) plus 50% glycerol. As control, flies expressing UAS-2xGFP with twi-Gal4 in mesodermal tissues were treated identically. They were then homogenized in lysis buffer and protein extracts were incubated with prewashed GFP beads (GFP-Trap_M; ChromoTek) for 2 h at 4°C. After incubation, the beads were washed three times with wash buffer (50 mM Tris-HCl, pH 8, 150 mM NaCl, 0.1% Triton X-100, and complete EDTA-free Protease inhibitor cocktail). Bound proteins were eluted by boiling in 2× SDS sample buffer and sent for mass spectrometry (Institute for Research in Immunology and Cancer proteomics center, Université de Montreal).

For immunoprecipitation, 150 adult fly thoraces were cut in half and incubated overnight in lysis buffer (50 mM Tris-HCl, pH 8, 150 mM NaCl, 1 mM EDTA, 0.5% Triton X-100, and complete EDTA-free protease inhibitor cocktail) plus 50% glycerol. They were then homogenized in lysis buffer and the homogenate was centrifuged twice for 20 min at 14,000 rpm in a 22R microfuge (Beckman Coulter) to remove debris and nonhomogenized myofibrils. The supernatant was incubated with prewashed anti-Flag beads (Sigma-Aldrich) for 2 h at 4°C. After incubation the beads were washed three times with wash buffer (50 mM Tris-HCl, pH 8, 150 mM NaCl, 0.1% Triton X-100, and complete EDTA-free protease inhibitor cocktail), and bound proteins were eluted in wash buffer containing 200 µg/ml of 3× Flag peptide (Sigma-Aldrich) for 1 h at 4°C. Then, the eluate was incubated with prewashed Ni-NTA agarose beads (QIAGEN) for 2 h at 4°C. After incubation the beads were washed three times with wash buffer and bound proteins were eluted by boiling in 2× SDS sample buffer and loaded on an 8% acrylamide gel. The following antibodies were used: rat anti–α-actinin MAC276, rat anti-actin MAC237, rat anti-myosin MAC147 at 1:2,000 (Babraham Bioscience Technologies), and mouse anti-Flag antibody at 1:5,000 (Sigma-Aldrich). The immunoreaction was visualized with ECL (GE Healthcare).

Binding of L.Lasp to thick filaments was measured by a cosedimentation assay as described previously (Burkart et al., 2007). In brief, IFM were dissected in relaxing solution with 0.5% Triton X-100 and protease inhibitors (Roche) from Act88F^{KM88} mutants, which lack thin filaments. IFM were separated into single myofibrils by pipetting and washed three times. Myofibrils were then homogenized in lysis buffer (10 mM Tris-HCl, pH 8, 50 mM NaCl, 2 mM MgCl$_2$, and 2 mM DTT). Soluble HisL.Lasp protein was purified from the lysate of sonicated cells on a Ni-NTA agarose column (GE Healthcare). The homogenate was incubated with or without 10 µM of purified HisL.Lasp for 1 h at RT under agitation. Centrifugation for 30 min at 30,000 rpm in an Optima Ultracentrifuge (Beckman Coulter) was used to separate pellet and supernatant. Samples were boiled in 2× SDS sample buffer, equally loaded on an 8% acrylamide gel and stained with Coomassie brilliant blue.

EM
Thoraces were treated with 5 mM MOPS, pH 6.8, 150 mM KCl, 5 mM EGTA, 5 mM ATP, and 1% Triton X-100 for 2 h at 4°C, followed by overnight incubation in the same buffer without Triton X-100 but 50% glycerol. This was repeated for a second time. Samples were then washed in rigor solution (5 mM MOPS, pH 6.8, 40 mM KCl, 5 mM EGTA, 5 mM MgCl$_2$, and 5 mM NaN$_3$) and fixed in 3% glutaraldehyde and 0.2% tannic acid in washing solution (20 mM MOPS, pH 6.8, 5 mM EGTA, 5 mM MgCl$_2$, and 5 mM NaN$_3$) for 2 h at 4°C. Samples were washed in washing solution, and then in 0.1 mM sodium phosphate, followed by a postfixation in ice-cold 1% osmium tetroxide in 0.1 mM sodium phosphate for 1 h at RT. Samples were washed in water and stained with 2% uranyl acetate for 1 h at 4°C. Finally, samples were washed in water, dehydrated in an ethanol series (30%, 50%, 70%, 90%, and 100%), and transferred into epoxypropane, before being embedded into epon-815 (Electron Microscopy

Sciences) and polymerized at 60°C for 48 h. Blocks were trimmed and cut into 90–100-nm-thick sections with an UltraCut E ultramicrotome (Reichert-Jung), put onto 150 mesh formvar-coated copper grids (Electron Microscopy Sciences), and stained with 4% uranyl acetate for 8 min and Reynold's lead for 5 min (both Electron Microscopy Sciences). Images were acquired at RT on a 12 BioTwin 120-kV transmission electron microscope (Tecnai) with an AMT XR80C CCD camera and EM-associated acquisition software (FEI). 50 images (from five different flies) were analyzed with ImageJ to determine myofibril area. For thick filament counts, we used 10 selected myofibrils out of five different flies.

Online supplemental material

Fig. S1 shows the *Lasp¹* mutant phenotype in BWM and TDT muscles. Fig. S2 shows EM sections of wild-type and *Lasp¹* mutant IFM at different ages and confocal images of IFM thin filaments of 18-d-old flies. Fig. S3 shows anti-Lasp antibody staining of wild-type BWM, TDT, and IFM muscles. Fig. S4 shows the rescue of larval *Lasp¹* phenotypes with different mutant Lasp proteins. Fig. S5 is a time-lapse series of FRAP experiment of L.LaspGFP in wild-type versus *Actn¹⁴* mutant larvae. Online supplemental material is available at http://www.jcb.org/cgi/content/full/jcb.201401094/DC1.

References

Bang, M.L., X. Li, R. Littlefield, S. Bremner, A. Thor, K.U. Knowlton, R.L. Lieber, and J. Chen. 2006. Nebulin-deficient mice exhibit shorter thin filament lengths and reduced contractile function in skeletal muscle. *J. Cell Biol.* 173:905–916. http://dx.doi.org/10.1083/jcb.200603119

Beall, C.J., M.A. Sepanski, and E.A. Fyrberg. 1989. Genetic dissection of *Drosophila* myofibril formation: effects of actin and myosin heavy chain null alleles. *Genes Dev.* 3:131–140. http://dx.doi.org/10.1101/gad.3.2.131

Björklund, A.K., S. Light, R. Sagit, and A. Elofsson. 2010. Nebulin: a study of protein repeat evolution. *J. Mol. Biol.* 402:38–51. http://dx.doi.org/10.1016/j.jmb.2010.07.011

Bullard, B., T. Garcia, V. Benes, M.C. Leake, W.A. Linke, and A.F. Oberhauser. 2006. The molecular elasticity of the insect flight muscle proteins projectin and kettin. *Proc. Natl. Acad. Sci. USA*. 103:4451–4456. http://dx.doi.org/10.1073/pnas.0509016103

Burkart, C., F. Qiu, S. Brendel, V. Benes, P. Hååg, S. Labeit, K. Leonard, and B. Bullard. 2007. Modular proteins from the *Drosophila sallimus* (*sls*) gene and their expression in muscles with different extensibility. *J. Mol. Biol.* 367:953–969. http://dx.doi.org/10.1016/j.jmb.2007.01.059

Chew, C.S., X. Chen, R.J. Bollag, C. Isales, K.H. Ding, and H. Zhang. 2008. Targeted disruption of the *Lasp-1* gene is linked to increases in histamine-stimulated gastric HCl secretion. *Am. J. Physiol. Gastrointest. Liver Physiol.* 295:G37–G44. http://dx.doi.org/10.1152/ajpgi.90247.2008

Gokhin, D.S., and V.M. Fowler. 2013. A two-segment model for thin filament architecture in skeletal muscle. *Nat. Rev. Mol. Cell Biol.* 14:113–119. http://dx.doi.org/10.1038/nrm3510

Katzemich, A., N. Kreisköther, A. Alexandrovich, C. Elliott, F. Schöck, K. Leonard, J. Sparrow, and B. Bullard. 2012. The function of the M-line protein obscurin in controlling the symmetry of the sarcomere in the flight muscle of *Drosophila*. *J. Cell Sci.* 125:3367–3379. http://dx.doi.org/10.1242/jcs.097345

Katzemich, A., K.A. Liao, S. Czerniecki, and F. Schöck. 2013. Alp/Enigma family proteins cooperate in Z-disc formation and myofibril assembly. *PLoS Genet.* 9:e1003342. http://dx.doi.org/10.1371/journal.pgen.1003342

Labeit, S., and B. Kolmerer. 1995. The complete primary structure of human nebulin and its correlation to muscle structure. *J. Mol. Biol.* 248:308–315. http://dx.doi.org/10.1016/S0022-2836(95)80052-2

Lee, S., L. Zhou, J. Kim, S. Kalbfleisch, and F. Schöck. 2008. Lasp anchors the *Drosophila* male stem cell niche and mediates spermatid individualization. *Mech. Dev.* 125:768–776. http://dx.doi.org/10.1016/j.mod.2008.06.012

Lehtokari, V.L., K. Pelin, M. Sandbacka, S. Ranta, K. Donner, F. Muntoni, C. Sewry, C. Angelini, K. Bushby, P. Van den Bergh, et al. 2006. Identification of 45 novel mutations in the nebulin gene associated with autosomal recessive nemaline myopathy. *Hum. Mutat.* 27:946–956. http://dx.doi.org/10.1002/humu.20370

Lu, S., S.L. Carroll, A.H. Herrera, B. Ozanne, and R. Horowits. 2003. New N-RAP-binding partners α-actinin, filamin and Krp1 detected by yeast two-hybrid screening: implications for myofibril assembly. *J. Cell Sci.* 116:2169–2178. http://dx.doi.org/10.1242/jcs.00425

McElhinny, A.S., C. Schwach, M. Valichnac, S. Mount-Patrick, and C.C. Gregorio. 2005. Nebulin regulates the assembly and lengths of the thin filaments in striated muscle. *J. Cell Biol.* 170:947–957. http://dx.doi.org/10.1083/jcb.200502158

Millevoi, S., K. Trombitas, B. Kolmerer, S. Kostin, J. Schaper, K. Pelin, H. Granzier, and S. Labeit. 1998. Characterization of nebulette and nebulin and emerging concepts of their roles for vertebrate Z-discs. *J. Mol. Biol.* 282:111–123. http://dx.doi.org/10.1006/jmbi.1998.1999

Nichols, S.A., W. Dirks, J.S. Pearse, and N. King. 2006. Early evolution of animal cell signaling and adhesion genes. *Proc. Natl. Acad. Sci. USA*. 103:12451–12456. http://dx.doi.org/10.1073/pnas.0604065103

Ottenheijm, C.A., C.C. Witt, G.J. Stienen, S. Labeit, A.H. Beggs, and H. Granzier. 2009. Thin filament length dysregulation contributes to muscle weakness in nemaline myopathy patients with nebulin deficiency. *Hum. Mol. Genet.* 18:2359–2369. http://dx.doi.org/10.1093/hmg/ddp168

Ottenheijm, C.A., H. Granzier, and S. Labeit. 2012. The sarcomeric protein nebulin: another multifunctional giant in charge of muscle strength optimization. *Front. Physiol.* 3:37. http://dx.doi.org/10.3389/fphys.2012.00037

Pappas, C.T., N. Bhattacharya, J.A. Cooper, and C.C. Gregorio. 2008. Nebulin interacts with CapZ and regulates thin filament architecture within the Z-disc. *Mol. Biol. Cell*. 19:1837–1847. http://dx.doi.org/10.1091/mbc.E07-07-0690

Pappas, C.T., P.A. Krieg, and C.C. Gregorio. 2010. Nebulin regulates actin filament lengths by a stabilization mechanism. *J. Cell Biol.* 189:859–870. http://dx.doi.org/10.1083/jcb.201001043

Pappas, C.T., K.T. Bliss, A. Zieseniss, and C.C. Gregorio. 2011. The Nebulin family: an actin support group. *Trends Cell Biol.* 21:29–37. http://dx.doi.org/10.1016/j.tcb.2010.09.005

Pelin, K., P. Hilpelä, K. Donner, C. Sewry, P.A. Akkari, S.D. Wilton, D. Wattanasirichaigoon, M.L. Bang, T. Centner, F. Hanefeld, et al. 1999. Mutations in the nebulin gene associated with autosomal recessive nemaline myopathy. *Proc. Natl. Acad. Sci. USA*. 96:2305–2310. http://dx.doi.org/10.1073/pnas.96.5.2305

Reedy, M.C., and C. Beall. 1993. Ultrastructure of developing flight muscle in *Drosophila*. I. Assembly of myofibrils. *Dev. Biol.* 160:443–465. http://dx.doi.org/10.1006/dbio.1993.1320

Reedy, M.C., B. Bullard, and J.O. Vigoreaux. 2000. Flightin is essential for thick filament assembly and sarcomere stability in *Drosophila* flight muscles. *J. Cell Biol.* 151:1483–1500. http://dx.doi.org/10.1083/jcb.151.7.1483

Root, D.D., and K. Wang. 1994. Calmodulin-sensitive interaction of human nebulin fragments with actin and myosin. *Biochemistry*. 33:12581–12591. http://dx.doi.org/10.1021/bi00208a008

Schönbauer, C., J. Distler, N. Jährling, M. Radolf, H.U. Dodt, M. Frasch, and F. Schnorrer. 2011. Spalt mediates an evolutionarily conserved switch to fibrillar muscle fate in insects. *Nature*. 479:406–409. http://dx.doi.org/10.1038/nature10559

Sparrow, J.C., and F. Schöck. 2009. The initial steps of myofibril assembly: integrins pave the way. *Nat. Rev. Mol. Cell Biol.* 10:293–298. http://dx.doi.org/10.1038/nrm2634

Steinmetz, P.R.H., J.E.M. Kraus, C. Larroux, J.U. Hammel, A. Amon-Hassenzahl, E. Houliston, G. Wörheide, M. Nickel, B.M. Degnan, and U. Technau. 2012. Independent evolution of striated muscles in cnidarians and bilaterians. *Nature*. 487:231–234. http://dx.doi.org/10.1038/nature11180

Suyama, R., A. Jenny, S. Curado, W. Pellis-van Berkel, and A. Ephrussi. 2009. The actin-binding protein Lasp promotes Oskar accumulation at the posterior pole of the *Drosophila* embryo. *Development*. 136:95–105. http://dx.doi.org/10.1242/dev.027698

Tanner, B.C., G.P. Farman, T.C. Irving, D.W. Maughan, B.M. Palmer, and M.S. Miller. 2012. Thick-to-thin filament surface distance modulates cross-bridge kinetics in *Drosophila* flight muscle. *Biophys. J.* 103:1275–1284. http://dx.doi.org/10.1016/j.bpj.2012.08.014

Tonino, P., C.T. Pappas, B.D. Hudson, S. Labeit, C.C. Gregorio, and H. Granzier. 2010. Reduced myofibrillar connectivity and increased Z-disk width in nebulin-deficient skeletal muscle. *J. Cell Sci.* 123:384–391. http://dx.doi.org/10.1242/jcs.042234

Wallgren-Pettersson, C., C.A. Sewry, K.J. Nowak, and N.G. Laing. 2011. Nemaline myopathies. *Semin. Pediatr. Neurol.* 18:230–238. http://dx.doi.org/10.1016/j.spen.2011.10.004

Witt, C.C., C. Burkart, D. Labeit, M. McNabb, Y. Wu, H. Granzier, and S. Labeit. 2006. Nebulin regulates thin filament length, contractility, and Z-disk structure in vivo. *EMBO J.* 25:3843–3855. http://dx.doi.org/10.1038/sj.emboj.7601242

Wright, J., Q.Q. Huang, and K. Wang. 1993. Nebulin is a full-length template of actin filaments in the skeletal muscle sarcomere: an immunoelectron microscopic study of its orientation and span with site-specific monoclonal antibodies. *J. Muscle Res. Cell Motil.* 14:476–483. http://dx.doi.org/10.1007/BF00297210

Zieseniss, A., A.G. Terasaki, and C.C. Gregorio. 2008. Lasp-2 expression, localization, and ligand interactions: a new Z-disc scaffolding protein. *Cell Motil. Cytoskeleton*. 65:59–72. http://dx.doi.org/10.1002/cm.20244